

On the effect of decreasing CO₂ concentration in the atmosphere

Isabella Bordi · Klaus Fraedrich · Alfonso Sutera ·
Xiuhua Zhu

Received: 29 October 2011 / Accepted: 29 October 2012 / Published online: 6 November 2012
© Springer-Verlag Berlin Heidelberg 2012

Abstract In the present paper the effect of an abrupt change of the atmospheric radiative forcing is investigated by means of a global climate model that includes a mixed layer ocean. In assessing if, under such a change, the model response has a bifurcation point, the steady solution is studied for a sudden decrease of CO₂ concentration from its actual value. It is found that there is a critical threshold for CO₂ content below which the model ends up to a snowball Earth. It occurs for a few percentage changes of CO₂ concentration around the threshold because the model strongly depends on the relationship among atmospheric temperature, water vapor content and the sudden ice-albedo feedback activation, even in the subtropical regions. Moreover, results suggest that the transition to ice-covered Earth is clearly favoured when Q-flux corrections (i.e. the parameterization of ocean heat transports) are removed.

Keywords Radiative forcing change · Hysteresis cycle · Global climate model · Energy balance model

1 Introduction

As known, the main contributors to the Earth's greenhouse effect are water vapor (including clouds), carbon dioxide, methane and ozone. Their contribution to the greenhouse effect depends on the characteristics of the gas, its

abundance and any indirect effects it may cause (Hartmann 1994). In the framework of a changing climate, the role played by CO₂ on the atmospheric radiative processes has attracted an increasing interest. A rough estimation of the radiative effect induced by this greenhouse gas can be provided by the following arguments. For a clear sky tropical atmosphere and when greenhouse gases are limited to water vapor, carbon dioxide and ozone, radiative transfer models, such as MODTRAN (Berk et al. 1989), predict that the outgoing long wave radiation at the top of the atmosphere (TOA) is about 290 Wm⁻² for CO₂ concentration of 360 ppm, 304 Wm⁻² for CO₂ concentration of 20 ppm, and 320 Wm⁻² for 0 ppm. Thus, the radiative effect of almost total CO₂ removal is 30 Wm⁻² and, in agreement with Lindzen (1995), about half of the effect occurs in the last 20 ppm.

The direct radiative effect of a decrease in CO₂ concentration may be amplified by the concomitant reduction of the water vapor content due to a drying atmosphere. In fact, if water vapor scale height is set to zero for CO₂ concentration of 20 ppm, MODTRAN computation suggests that the atmosphere would lose about 368 Wm⁻² toward the outer space (compared to 304 Wm⁻² mentioned before, a value very close to the incoming radiation at tropical latitudes). In the circumstance in which the outgoing long wave radiation exceeds the incoming solar, it would be possible that the surface temperature drops below freezing, so that sea ice may form. The question is whether the sea ice will extend even to tropical regions. In this case, the insulating effect of ice would almost completely cut ocean heat fluxes and a sufficiently large evaporation, which strongly controls the surface heat budget, so that the steady state would be irreversibly locked in a permanent snowball, unless (perhaps unreasonable) large amount of greenhouse gases is injected, later on, into the atmosphere.

I. Bordi (✉) · A. Sutera
Department of Physics, Sapienza University of Rome,
Rome, Italy
e-mail: Isabella.bordi@roma1.infn.it

K. Fraedrich · X. Zhu
Universität Hamburg, KlimaCampus, Hamburg, Germany

This should be because the atmosphere has lost the main component of the greenhouse effect (i.e. the water vapor) and the other greenhouse gases might not be able to compete with the ice-albedo feedback. Hence, the ice-albedo feedback, triggered by the water vapor content variation, might be crucial in determining the reversibility of the ice-covered Earth state. These features have to be addressed more quantitatively than on the basis of the simplified arguments discussed so far.

Recently, Voigt and Marotzke (2010) used the coupled atmosphere–ocean general circulation model (GCM) ECHAM5/MPI-OM to investigate the transition from the present-day climate to a modern (present land mass distribution) snowball Earth. By applying an abrupt decrease of the total solar irradiance (TSI), they found the critical TSI marking the snowball Earth bifurcation point, and, more importantly for our purposes, they noted that the transition to the modern snowball Earth can be obtained by keeping TSI at its present-day value but setting the atmospheric CO₂ concentration to 0.1 % of its pre-industrial value. Differently, Lacis et al. (2010), by zeroing out the whole non-condensing greenhouse gases in a GCM with a mixed layer ocean, found that even though the global surface temperature becomes colder than -21 °C, incident solar radiation is sufficient to keep about one half of the ocean ice-free. The simulation carried out using a coupled atmosphere–ocean GCM confirmed this result. Also, Held et al. (2010) studied the fast and slow components of the global warming by returning abruptly to the preindustrial CO₂ forcing, but the possible transition to the ice-covered Earth has not been investigated. The snowball Earth state, in fact, has been widely studied along the years for Neoproterozoic (Hoffman et al. 1998; Crowley et al. 2001; Donnadieu et al. 2004; Le Hir et al. 2007; Micheels and Montenari 2008, Le Hir et al. 2010 just to mention a few, see also references therein) and no specific efforts have been made to analyze the transition to a modern snowball state induced by an abrupt CO₂ decrease. Thus, the issues concerning the CO₂ threshold for a transition to a modern snowball Earth, the reversibility of such a state, and the impact of ocean energy transports are still open questions that need further investigation. These will be topics of the present paper. In our view, these kind of analyses, even though they appear of less interest for the low occurrence probability of such a state, represent an important challenge for scientists and climate modellers for improving their understanding on the Earth's climate and favoring a deep comparison among GCMs.

We could try to discuss the proposed subjects by means of a radiative convective model as in Rondanelli and Lindzen (2010), but we would miss the ocean response to radiative forcing, preventing the assessment of the role played by the ice-albedo feedback and the ocean heat

fluxes. Thus, we used the GCM with a mixed layer ocean developed by the University of Hamburg (Planet Simulator, hereafter PlaSim). Despite some heavy simplifications, especially those concerning the radiative non-condensing species (only CO₂ and O₃ are considered) and the slab ocean, PlaSim simulates a reasonable present climate. These limitations may appear an over simplification, however, by drastically reducing the parameter space, it pays off. Also, since Lacis et al. (2010) obtained similar results using a GCM with a slab ocean and a GCM coupled with a dynamic ocean, we feel enough confident on the capability of PlaSim in representing the features under investigation.

In particular, the present paper addresses the following questions: (1) the climate response to a sudden reduction of CO₂ concentration and the existence of a threshold for the transition to the modern snowball Earth; (2) the role played by the ocean vertical/meridional heat transports in determining the global mean surface temperature under such a change of the greenhouse gas. The first question (Sects. 3.1 and 3.2) is motivated by the different climate responses obtained in previous studies quoted above when CO₂ concentration is drastically removed or at least reduced to a small amount, but it is far from our intention to carry out a stringent comparison with them. Models used in fact are different (though parameter settings are almost the same) and it is hard to properly establish the origin of the detected differences. Then, the paper moves to check the role of the slab ocean (Sect. 3.2). In Sect. 4, the capability of the zero-dimensional Budyko-Sellers type model (Budyko 1969; Sellers 1969) in capturing the main features of the climate response provided by PlaSim, is investigated. That is to complement the results obtained, offering some speculations on the PlaSim solutions. Conclusions are provided in the final section.

2 The model set up

The Planet Simulator (Fraedrich et al. 2005a; freely available under <http://www.mi.uni-hamburg.de/plasim>) is a climate model with the Q-flux ocean and a mixed-layer of a given depth. In previous studies the model has been used to analyze the effect of vegetation extremes of a desert world versus green planet (Fraedrich et al. 2005b), the entropy budget and its sensitivity (Fraedrich and Lunkeit 2008), the global energy and entropy budget in a snowball Earth hysteresis (Lucarini et al. 2010), and the double ITCZ dynamics in an aquaplanet setup (Dahms et al. 2011). This model is being employed to reconstruct historic climates (Grosfeld et al. 2007), to determine the younger history of the Andean uplift (Garreaud et al. 2010), to analyse the effect of mountains on the ocean circulation (Schmittner

et al. 2011), and to evaluate biogeophysical feedbacks (Dekker et al. 2010). Furthermore, it enables investigations of climates very different from recent Earth conditions as shown in applications for Mars with and without ice (Stenzel et al. 2007), the Neoproterozoic snowball earth (Micheels and Montenari 2008), and the Permian climates (Roscher et al. 2011). Recent studies have investigated the effects of O₃ removal (Bordi et al. 2012a) and CO₂ change at different rates (Bordi et al. 2012b) on the model response.

The primitive equations formulated for vorticity, divergence, temperature and the logarithm of surface pressure are solved via the spectral transform method (Orszag 1970; Eliassen et al. 1970). The parameterizations for unresolved processes consist of long (Sasamori 1968) and short (Lacis and Hansen 1974) wave radiation. That is, the model takes into account only water vapor, carbon dioxide and ozone as greenhouse gases. Computations of their transmissivities are taken from Sasamori (1968). The ozone concentration is prescribed according to the analytic ozone vertical distribution of Green (1964). The annual cycle and the latitudinal dependence are introduced. Further parameterizations are included for interactive clouds (Slingo and Slingo 1991; Stephens 1978; Stephens et al. 1984), moist (Kuo 1965, 1974) and dry convection, large-scale precipitation, boundary layer fluxes of latent and sensible heat and vertical and horizontal diffusion (Laursen and Eliassen 1989; Louis 1979; Louis et al. 1982; Roeckner et al. 1992). The land surface scheme uses five diffusive layers for the temperature and a bucket model for the soil hydrology. The ocean is represented by a mixed layer (swamp) ocean, which includes a 0-dimensional thermodynamic sea ice model. The slab ocean model consists of a prognostic equation at each ocean point for the oceanic mixed layer temperature T_{mix} , that is:

$$\frac{\partial T_{mix}}{\partial t} = \frac{Q_A + Q_O}{\rho_w c_{pw} h_{mix}} \quad (1)$$

where ρ_w is the density, c_{pw} the heat capacity of ocean water, h_{mix} is the ocean mixed layer depth, Q_A the net atmospheric heat flux into the ocean, and Q_O the ocean mixed layer heat flux (oceanic transport and deep water exchange). As commonly done, Q_O is prescribed from monthly mean data which are obtained from climatology of the uncoupled (i.e. prescribed SST) model simulation. We wish to notice the crucial role played by Q_O (see Zhu et al. 2006, 2010); in a comprehensive ocean–atmosphere model this term, in fact, may lead to long-term memory and/or interannual variability of the ocean circulation. The parameterization here employed instead, limits these additional time scales in a particular climate regime. The consequence of this will be illustrated in a coming section. The 0-dimensional thermodynamic sea-ice model of Semtner

(1976) is included: sea ice is formed if the ocean temperature drops below the freezing point, set to 271.25 K, and is melted whenever the ocean temperature increases above this point.

The prescribed surface albedo R_s for open water is set to a default value of 0.069. For sea ice it is given as a function of the ice surface temperature T_i :

$$R_s = \min(R_s^{\max}, 0.5 + 0.025(273 - T_i)) \quad (2)$$

where the prescribed maximum sea ice background albedo R_s^{\max} is set to a default value of 0.7.

For snow-covered areas the background albedo R_s^{clim} is modified to give the actual albedo R_s which is used in the radiation scheme. R_s is given by:

$$R_s = R_s^{clim} + (R_s^{snow} - R_s^{clim}) \frac{z_{snow}}{z_{snow} + 0.01} \quad (3)$$

where z_{snow} is the snow depth and R_s^{snow} is the albedo of the snow that depends on the surface temperature T_s as:

$$R_s^{snow} = R_{\max}^{snow} + (R_{\min}^{snow} - R_{\max}^{snow}) \left(\frac{T_s - 263.16}{10} \right) \quad (4)$$

with $R_{\min}^{snow} \leq R_s^{snow} \leq R_{\max}^{snow}$ and default values $R_{\min}^{snow} = 0.4$ and $R_{\max}^{snow} = 0.8$.

The PlaSim is used here in T21 horizontal resolution (approx. $5.6^\circ \times 5.6^\circ$ on the corresponding Gaussian grid) with 10 sigma levels in the vertical. The present day climate is reasonable considering the coarse resolution and relative simplicity of the model compared with a state-of-the-art GCM. Also, the globally averaged energy fluxes are in good agreement with observations (Kiehl and Trenberth 1997). Larger differences (more than 10 %) can be noted in the sensible and latent heat flux where PlaSim shows lower (sensible) and higher (latent) heat fluxes than observed. As the water vapor greenhouse effect is a relevant feature of the subsequent analysis, the global water cycle as represented by the PlaSim control run is shown in Fig. 1. The figure describes continental and oceanic precipitation, evaporation and transports by the atmosphere and river runoff (units in $\text{kg m}^{-2} \text{year}^{-1}$). There is agreement with observations (Trenberth et al. 2006): precipitation and evaporation over the ocean (precipitation: 470 compared to 373, evaporation: 505 and 413) and over the continents (precipitation: 142 compared to 113, evaporation: 107 and 73) are overestimated by PlaSim, while atmospheric transport and surface runoff are slightly underestimated (35 compared to 40). Moreover, the low spatial resolution here employed may underestimate some teleconnections such as the ones described in Zhu et al. (2011).

The present study consists of simulations which, starting from the control run, are performed by a set of time-dependent greenhouse gas related forcings: (1) switching off CO₂ and O₃ concentrations with ocean mixed layer

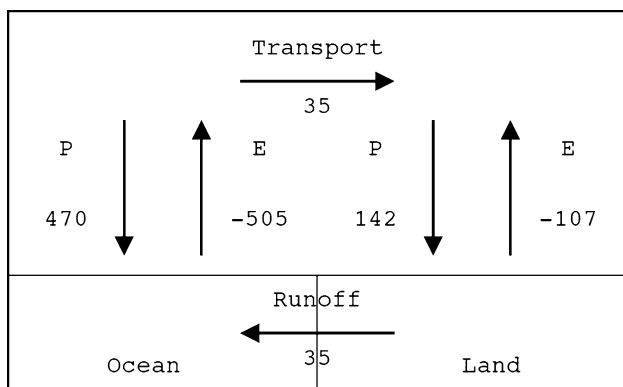


Fig. 1 PlaSim global and annual mean water budget (units in $\text{kg m}^{-2}\text{year}^{-1}$)

depth of 50 m and 250 m; (2) instantaneously decreasing the CO_2 content to 30 and 20 ppm and then, after 200 years, abruptly increasing it to 2,000 ppm; (3) an instantaneous decrease of CO_2 content to 30 ppm without Q-flux corrections. The setup for the control run is given by the actual O_3 distribution, the present CO_2 content (360 ppm), and the mixed layer depth of $h_{\text{mix}} = 50$ m.

3 The planet simulator analysis

In this section, we describe the main results obtained using the PlaSim in investigating the transition to ice-covered Earth induced by a sudden CO_2 decrease and the role played by Q-fluxes.

3.1 Effect of sudden CO_2 removal

Let us consider the Planet Simulator described in Sect. 2. We have computed the equilibrium solution for $\text{CO}_2 = 360$ ppm that, in our framework, represents the present climate. Then, we have instantaneously removed both CO_2 and O_3 . It is worth noticing that in the present model O_3 must be removed if CO_2 concentration is set to zero, otherwise the stratospheric warming effect of O_3 would lead to an unstable solution causing a model blow up. CO_2 stratospheric cooling, in fact, would no longer be able to compensate the O_3 warming. By setting the mixed layer depth at 50 and 250 m, respectively, we have summarized the model results as in Fig. 2.

In agreement with Lacis et al. (2010) and MODTRAN, the initial imbalance due to CO_2 and O_3 removing at TOA is about $40\text{--}50 \text{ Wm}^{-2}$, about 30 Wm^{-2} due to CO_2 and the rest to O_3 . However, at variance with Lacis et al. (2010), but in agreement with Voigt and Marotzke (2010), we get in both cases a snowball Earth. This may be due to differences in the models used, different Q-flux structure, or other different model features that may hardly be identified. Other

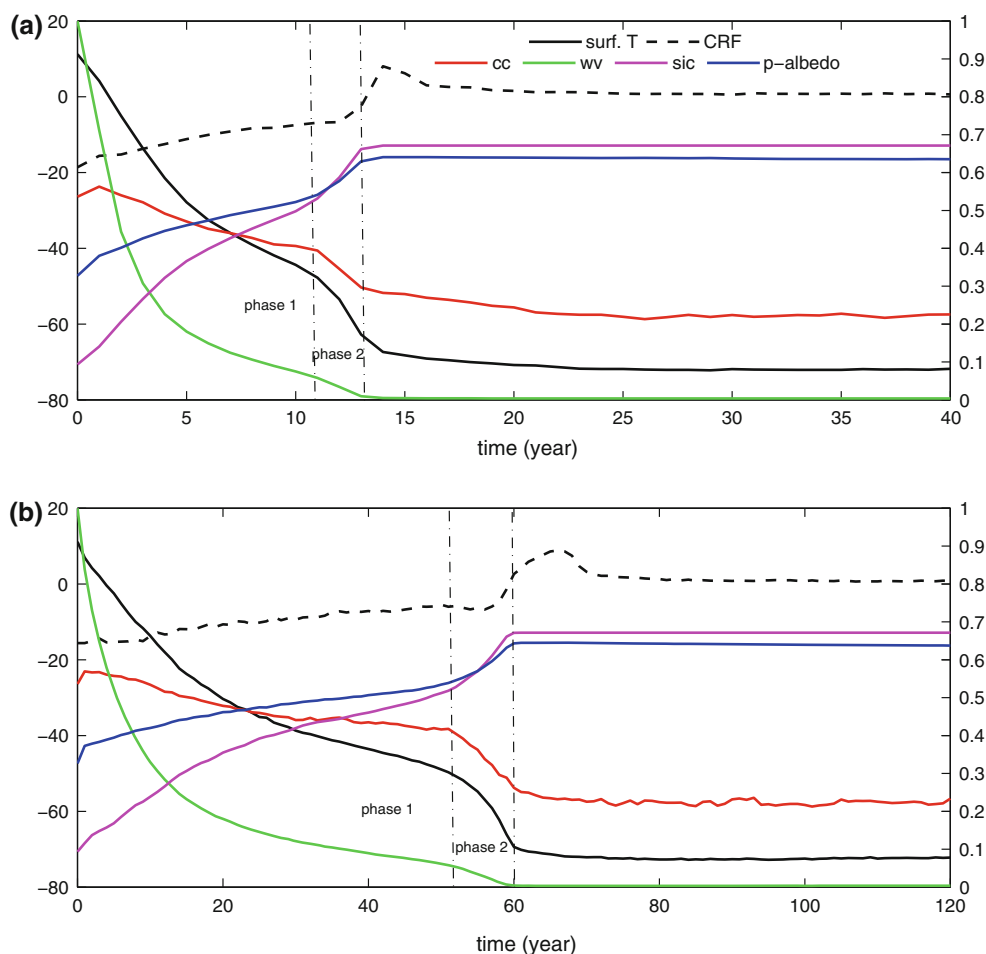
differences are found in the cloud cover behavior that, in our case, is decreasing in time because of the drastic reduction of the atmospheric water vapor, while in Lacis et al. (2010), it is increasing. These features appear robust with respect to the ocean depth. Nevertheless, our results suggest that in the absence of non-condensing greenhouse gases the planet described by our model has two clearly distinct features: (1) a first phase from the time of switch-off to a time, depending on the depth of the passive ocean, where the rate of change of the parameters appears to follow a slow linear response to the induced forcing perturbation (of the order expected by merely computing the radiative response), and (2) a second phase characterized by a faster response, seemingly nonlinear, leading to the transition to the snowball state. To be noted is the rapid decrease of water vapor content associated with an increase of both sea-ice cover and planetary albedo, a feature that suggests the activation at global scale of the ice-albedo feedback discussed in the introduction. It seems that the activation of such a feedback provides the transition to the snowball state. The difference between TOA net fluxes for cloudy and clear sky conditions, suggests that the cloud radiative forcing (CRF) is active mainly during the first phase of the model response, before the drastic reduction of water vapor content and cloud cover. It is worth noting that the transition to the ice-covered state may occur even earlier in the model if a stochastic forcing would be applied, as it has been shown in Fraedrich (1978) or Sutera (1981).

3.2 Transition to modern snowball earth

Motivated by the above findings, we have investigated if there is a critical value for CO_2 concentration that leads to the snowball Earth transition. After some trial and error, we found that $\text{CO}_2 = 20$ ppm is a rough estimate of such a critical value (note that, according to MODTRAN calculations previously discussed, 20 ppm provides about half of the total contribution of CO_2 to the greenhouse radiative forcing). Above this value, the model, although reaching very cold global average temperatures, would exhibit ice-free subtropics with reasonably warm temperatures. The critical value was determined by setting the O_3 concentration to the same value of the control run. As an example, we show the same diagnostics above for two values of CO_2 content, namely 20 ppm and 30 ppm, respectively.

1. First, let us analyze the case of 20 ppm. The model behavior is displayed in Fig. 3a. If we consider the first 200 model years, the model will be in a snowball Earth regime from year 170–200. To test if, in these conditions, a sudden increase of CO_2 to 2,000 ppm (a tenfold increase) would restore an ice-free Earth, after year 200 we set CO_2 content to this value.

Fig. 2 Time evolution of global annual mean (not area weighted) surface temperature (surf. T), cloud radiative forcing (CRF), cloud cover (cc), column water vapor content (wv), sea ice cover (sic) and planetary albedo (p-albedo) after zeroing out both CO₂ and O₃ contents: **a** ocean mixed layer depth $h_{mix} = 50$; **b** $h_{mix} = 250$ m. Surface temperature and CRF follow the *left axis*, while the other variables the *right axis*. Units for surface temperature and CRF are °C and Wm⁻², respectively. Water vapor content is normalized with respect to the equilibrium value of the control run. Vertical dash-dot lines denote the first and second phase of the model solutions



We gained a modest temperature rise with an equally modest flux imbalance at TOA, which leads to the inference that such a state appears to be an irreversible one, at least in the range of the forcing variation considered. In illustrating the overall structure of the model solution, we show the time-latitude diagram of the zonal mean surface temperature for this run (Fig. 3b). The time behavior of the temperature field clearly shows that the gentle slope of the temperature decreasing in the first 150 years is quickly replaced by a sudden cooling, mainly driven by the Southern Hemisphere (SH), leading to the snowball Earth. At the new equilibrium, the surface albedo (not shown) averaged over the SH is higher than the one over the Northern Hemisphere (NH; about 0.68 against 0.6), suggesting that the asymmetry between the two hemispheres in the sea ice plays a key role in establishing the snowball state. The result appears consistent with that of Voigt and Marotzke (2010) when CO₂ concentration is set to 0.1 % of its pre-industrial value. Also the transition time to the modern snowball Earth is similar, i.e. about 200 years in our case against about 240 years found by Voigt and Marotzke (2010).

In our case, despite the large long wave radiative forcing applied at year 200, the temperature response is so small that not appreciable change of state is noticed. The ice-albedo feedback, in fact, is so dominating that the system remains in a close neighbor state. It should be noted that Marotzke and Botzet (2007) found a similar result studying the transition back from an ice-covered Earth state induced by an abrupt decrease to near-zero TSI. The authors showed that by setting today's TSI and 10 times today's atmospheric CO₂ level (3,480 ppm) only a small ice retreat and some reduction in total ice volume can be obtained; about 100 times today's atmospheric CO₂ concentration was necessary to break-up the complete ice-covered state. The latter result is also obtained using the PlaSim by abruptly increasing CO₂ concentration to 36,000 ppm at year 200: the model solution (here not shown) rapidly converges to ice-free conditions. In the tropics and mid-latitudes, when the snowball state is established, the temperature lapse rate is reduced but still present (not shown). Moreover, the tropopause height is lower suggesting that heat transports by baroclinic eddies are more active. In polar region, instead, the temperature profiles become almost isothermal. Thus, as discussed by Pierrehumbert

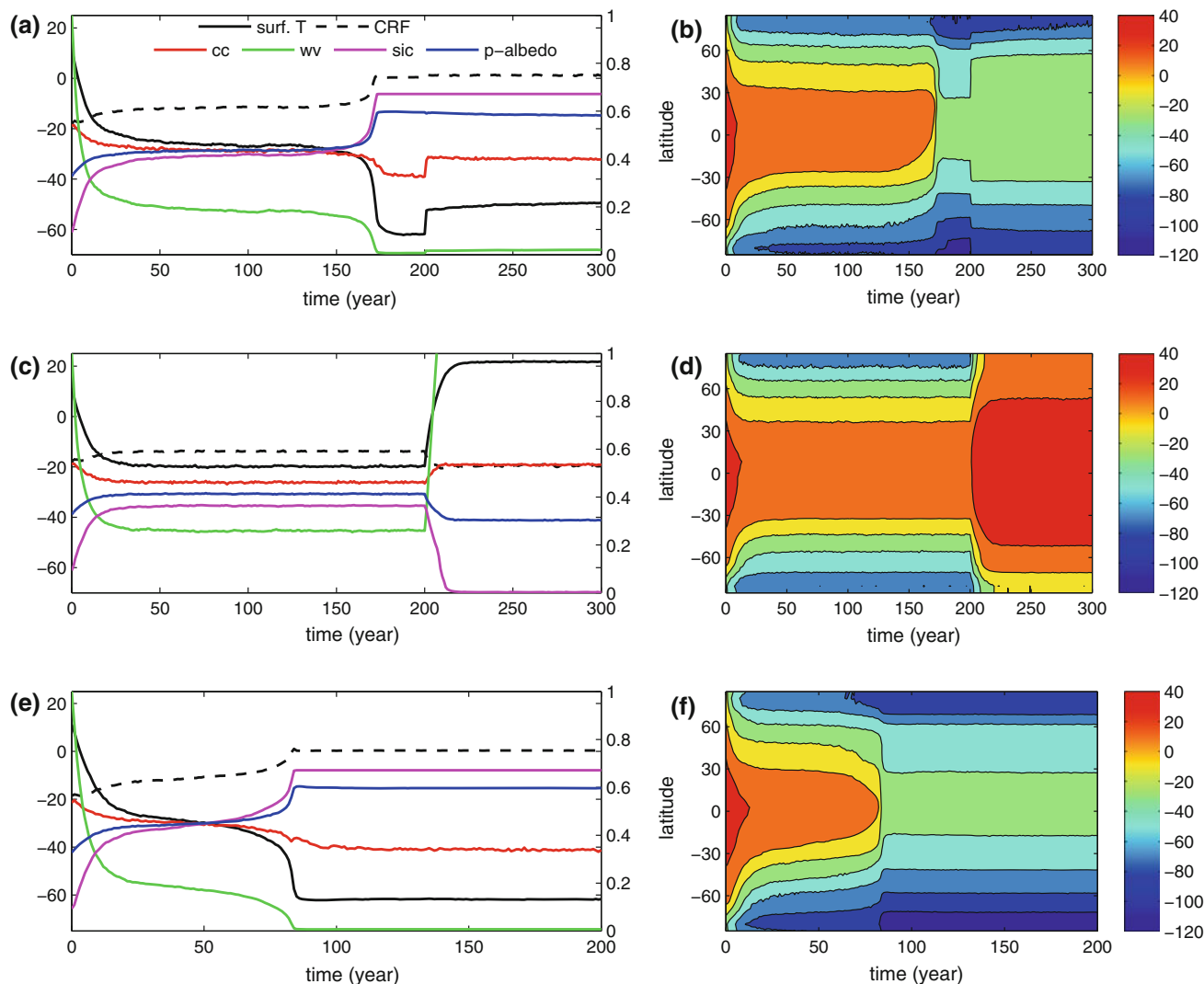


Fig. 3 As in Fig. 2a but with actual ozone content and **a** $\text{CO}_2 = 20 \text{ ppm}$ till year 200, then $\text{CO}_2 = 2,000 \text{ ppm}$, **c** $\text{CO}_2 = 30 \text{ ppm}$ till year 200, then $\text{CO}_2 = 2,000 \text{ ppm}$, and **e** $\text{CO}_2 = 30 \text{ ppm}$ but without

Q-fluxes. The contour plots on the right (**b**, **d**, **f**) refer to zonal mean surface temperature as a function of time for the cases shown in **a**, **c**, **e**, respectively. Units are $^\circ\text{C}$

et al. (2011), in the snowball state the efficiency of the greenhouse effect is strongly reduced, inhibited both by the temperature lapse rate decrease and drying of the atmosphere, but in our case there is chance of triggering the exit from the snowball state. This is the reason why a very large CO_2 amount is needed for deglaciation.

It is worth noting that the CO_2 concentration of 36,000 ppm corresponds to about 0.04 bar which is much lower than the thresholds found by some authors for deglaciation (see for example Caldeira and Kasting 1992 or Pierrehumbert 2005). We like to point out that such a value for CO_2 amount is not a “threshold for deglaciation” since different concentrations between 360 and 36,000 ppm have not been tested (being out of the scope of this study). Despite this caveat, the detected discrepancy might be due to the different geographical distribution of continents that

affects climate through surface albedo, to the differences in the model parameterizations (precipitation, clouds, snow/ice schemes), or to the model sensitivity to the greenhouse effect and longwave cloud radiative forcing when CO_2 is increased (for discussion see for example Hu and Yang 2010 and references therein). All these factors, including the different vertical structure of the temperature field at the snowball state mentioned above, prevent us from performing a stringent comparison with previous results largely documented in the literature.

Moreover, we notice that also Romanova et al. (2006) investigated the effect of CO_2 change in producing extreme climates. The authors, using a previous version of PlaSim with five sigma-levels, considered six CO_2 values ranging from 1 ppm to 1,440 ppm and analysed the model responses. They found that low values of CO_2 concentration

(1, 10 and 25 ppm) are not sufficient to cause a full glaciation of the planet. The origin of the discrepancy with present results might be due to: (1) the improvements applied to the model in the recent years (mainly concerning the precipitation scheme), or (2) the interpretation of the model solution provided by Romanova et al. (2006). In that case, the experiments, “integrated over 50 years when they reach the equilibrium state”, might refer to the first phase of the model response, which lasts for many decades (about 150 years) before the transition to the snowball state and, therefore, can be confused with a steady state. The last hypothesis seems to be supported by the values of the planetary albedo and the spatial distribution of sea ice shown by Romanova et al. (2006), their Fig. 5) that appear consistent with the results obtained here during the first phase of the model solution (Fig. 3a).

2. Next, let us consider the same set up as before but $\text{CO}_2 = 30$ ppm. Results are summarized in Fig. 3c. For the first 200 years, the model behavior, apart for cloud cover, shows features similar to those illustrated by Lacis et al. (2010), namely there is a single time scale that controls the whole of the parameters reported in the figure. In particular, we notice that the sea ice extension averages to 35 % of the globe, strongly contrasting with the previous case where this quantity almost reaches the 67 % limit. Moreover, the switch on of 2,000 ppm CO_2 concentration leads to a very warm world, leading to the conclusion that, in this model, as long as the subtropics are ice-free, an accumulation of CO_2 will restore warm climate conditions. To better illustrate this result, we present the time-latitude behavior of the zonal mean temperature in Fig. 3d: very warm temperatures extend beyond the tropics after year 200 (i.e. at the switch on of 2,000 ppm) and persist there on.

Summarizing, despite the differences in many aspects between this model and others, we reached similar conclusions: as long as the subtropics are ice-free, radiative perturbations alone are capable of maintaining the model climate far from a snowball Earth. In the present model, these warm tropics are maintained by the combined effect of greenhouse gases and solar fluxes. In view of the uncertain parameterization of clouds, it could be possible that high cirrus clouds, which are known to be transparent to solar fluxes but opaque to infrared fluxes, might provide a similar infrared warming as in Rondanelli and Lindzen (2010).

However, in this picture, there is a caveat we like to mention, which is related to the role of Q-fluxes that are the simplistic form to couple the ocean and the atmosphere. The question is whether the radiative perturbation alone may drive the global mean surface temperature towards the

modern snowball Earth. In addressing the effect of Q-fluxes there is not a better way than to analyze the model behavior at a given CO_2 content and excluding these fluxes. For $\text{CO}_2 = 30$ ppm results are presented in Fig. 3e, f. Unlike what has been obtained before at this CO_2 concentration (Fig. 3c, d), the snowball Earth appears to be the asymptotic solution. Therefore, the result suggests that the details of the ocean circulation are important driving features as discussed by Winton (2003). Such an aspect requires a cautious interpretation of the conclusions, which are merely based on a passive ocean, or, alternatively, a highly parameterized one. Similar experiments should be carried out using a coupled atmosphere–ocean GCM. Nevertheless, we are allowed to speculate that the climate state is not simply driven by the radiative forcing because the ocean–atmosphere heat fluxes play a crucial role.

As a final remark, we notice that the asymmetry between the two hemispheres, which appears in all model solutions displayed so far and is further investigated in the following section, seems to suggest the key role played by the heat and momentum transports in determining the nature of the modeled general circulation as investigated in several studies (see for example Bordi et al. 2004; 2007).

4 A simple underlying energy balance model

In this section we attempt to reduce the degrees of freedom of PlaSim by employing a simpler energy balance model, which may help to illustrate the main features presented above. In particular, we wish to account for:

1. Two different time scales observed before reaching what appears to be a bifurcation point and thereafter;
2. Back-transition from the modern snowball Earth when the CO_2 concentration is set to very large values keeping the solar constant at the present value;
3. The radiative perturbation related to the latitude of the ice margin;
4. Hemispheric asymmetry: The radiative effect cools one hemisphere more than the other, as observed in PlaSim simulations.

The energy balance model approach is introduced followed by its analysis and interpretation of the model experiments.

4.1 Two time scales near bifurcation

By looking Fig. 3a, it appears that the source of transition from the control to the snowball state is the change in the planetary albedo. When the surface temperature crosses the threshold temperature for ice formation (about 271 K), an increase of the albedo occurs. In the model, the ice albedo

is computed by interpolating between 0.5 and 0.7 as a function of the ice surface temperature. On the other hand, the mean value of the planetary albedo in the control run is about 0.3, while after the time of the CO₂ reduction to 20 ppm it increases up to about 0.6–0.7 (values approaching 0.7 are found in the SH due to the greater sea ice cover compared to the NH). The first planetary albedo change occurs when the global mean surface temperature is about 263 K (Fig. 3a). A model that well captures this behavior is the surface energy balance of Budyko-Sellers (Budyko 1969; Sellers 1969). Budyko (1969) used an albedo stepwise dependent on the surface temperature, with a given threshold (about the same temperature of PlaSim). Although we are aware that in the present climate the energy balance at the surface is mainly controlled by solar energy and evaporation, in view that at the low temperatures where the ice-albedo feedback is active there is little evaporation left, the energy balance seems more related to the short and long wave radiation. Thus, the simplest energy balance model (EBM) aping PlaSim is:

$$C \frac{d}{dt} T_s = S_0 [1 - \alpha(T_s)] - \varepsilon \sigma T_s^4 \quad (5)$$

where C , T_s , S_0 , α , ε and σ are the ocean heat capacity, the surface temperature, the annual global mean amount of solar radiation reaching the top of the atmosphere, the planetary albedo, the infrared opacity of the atmosphere, and the Stefan-Boltzmann constant, respectively. The EBM proposed here is based on the equation for T_s where the outgoing longwave radiation (OLR) is expressed as a function of the surface temperature and the opacity of the atmosphere; differently from the EBM discussed in Pierrehumbert et al. (2011), where the clear-sky ORL is computed by an atmospheric radiation model and represented by a low-order polynomial fit, no specific assumptions are made on the vertical profiles of temperature and humidity.

It should be noted that if the latitudinal dependence of S_0 is taken into account, some heat flux should be expected because motion ensues that might change the ocean's heat content, the heating distribution, or both. We shall return to this point later on.

For a climate steady state, the knowledge of T_s will allow estimating the atmosphere opacity by knowing S_0 and α . As an example, let us consider $S_0 = 340 \text{ Wm}^{-2}$ and for the present climate $\alpha = 0.3$ and $T_s = 288 \text{ K}$; for these values $\varepsilon = 0.61$. For a snowball Earth, instead, let us suppose $\alpha = 0.7$ and $T_s = 211 \text{ K}$ (just about the value reached by the PlaSim after the transition to the snowball Earth); the steady solution of (5) provides $\varepsilon = 0.9$. It is found that the difference in infrared emission is about 130 Wm^{-2} (which is about what occurs in PlaSim). Since, by instantaneously decreasing CO₂ to 20 ppm, we increase the

long wave emission of the atmosphere by just 15 Wm^{-2} , the rest to reach a snowball Earth has to be provided by other greenhouse gases, namely water vapor.

Thus, it is of interest to analyze the time-dependent solution of T_s obtained by integrating Eq. (5). Let us consider the initial value of ε be 0.61 and increase it up to 0.9 at a given time rate to mimic the long wave radiative effect of the CO₂ reduction to 20 ppm where the transition to snowball Earth occurs. Moreover, let be $S_0 = 340 \text{ Wm}^{-2}$, $C = 7 \text{ Wm}^{-2} \text{ K}^{-1} \text{ year}$ (the ocean heat capacity estimated for an ocean depth of 50 m) and the albedo a hyperbolic tangent function of T_s , ranging from 0.3 to 0.7 (see Table 1). The transition from low albedo values to the higher value of 0.7 occurs for T_s crossing the threshold of $-20 \text{ }^\circ\text{C}$. For this parameter setting, the time-dependent solution of Eq. (5) is that shown in Fig. 4. As can be noted the surface temperature (after adjusting to perturbation) decreases almost linearly from its initial value of about $15 \text{ }^\circ\text{C}$ toward about $-10 \text{ }^\circ\text{C}$ and then, when it crosses the threshold of the major albedo change at $-20 \text{ }^\circ\text{C}$, it quickly decreases to about $-60 \text{ }^\circ\text{C}$. The latter will be the equilibrium temperature if all parameters are kept constant from then on. From a qualitative comparison of Fig. 3a (first 200 years) with Fig. 4, it emerges that the simple EBM is able to capture the basic features of the surface temperature behavior provided by PlaSim, i.e. the two different time scales characterizing the temperature decline. The first part of the temperature decline appears to be related to the change of the opacity ε and the sharp increase of the planetary albedo, while the second is mainly controlled by the rapid change of the planetary albedo toward its higher value (ice-albedo feedback).

4.2 Back transition from snowball earth

Now, let us investigate the second question concerning the transition back from the ice-covered Earth state. As is well known, for the model described by (5) there is a range of the parameter ε (or S_0) wherein the two stable solutions snowball Earth and more temperate planet co-exist. This range depends on both the threshold temperature at which the planetary albedo changes and the sharpness of this transition. In order to illustrate these features, we present in Fig. 5 the steady states (T_s) of the EBM when ε is varied

Table 1 Parameter setting used for computing the time behavior of T_s by integrating Eq. (5) with ε varying linearly from 0.61 to 0.9 (Fig. 4)

| S_0 (Wm^{-2}) | α (dimensionless) | C ($\text{Wm}^{-2} \text{ K}^{-1} \text{ year}$) |
|----------------------------|--|--|
| 340 | $0.5 + 0.2 \tanh((-20 - T_s)/10)$ with T_s in C | 7 |

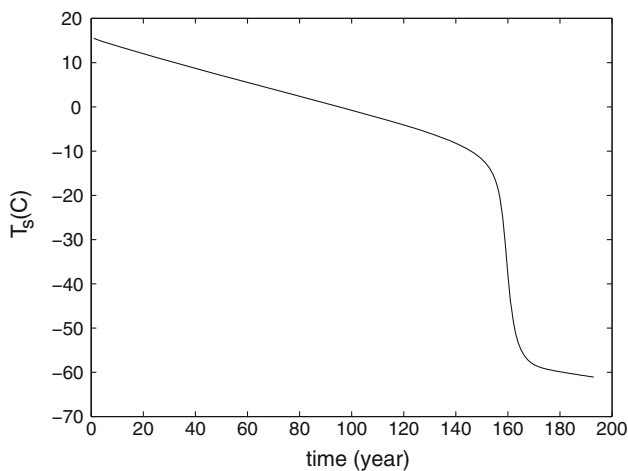


Fig. 4 Time evolution of the surface temperature T_s obtained by integrating the 0-dimensional energy balance model Eq. (5) for the opacity ϵ varying linearly from 0.61 to 0.9. The parameters settings are listed in Table 1

back and forth within the interval 0.2–0.9. Black line in the figure is obtained by parameterizing the planetary albedo as a step function of values 0.3 and 0.7, with the transition between these boundary values occurring at the threshold surface temperature $T_t = -10$ °C. Blue and red lines, instead, correspond to the albedo parameterized through a hyperbolic tangent function centered at $T_t = -10$ °C and $T_t = -20$ °C, respectively (see Table 2). The figure shows the predictive value of the EBM. It shows that if the system is in a snowball state, and if we increase a greenhouse gas

such as CO_2 , we might escape from this state provided that the associated radiative forcing ϵ reaches the threshold value identified by the lower branch of the hysteresis curves shown in Fig. 5. Moreover, it is predicted that the new state will be a great deal warmer than what is expected because we must add also the water vapor effect that dominates once the evaporation has been re-established. This behavior involves the insulating nature of ice that has been discussed in the context of long-term climate change by Saltzman and Sutera (1984). Also, it is worth noticing that the rate of approach to the two steady state branches is just a consequence of the sharpness of the albedo change associated with the ice-albedo feedback activation or deactivation. In particular, from Fig. 5 (red line) it is found that the transition from the snowball Earth to ice-free solution can occur for $\epsilon = 0.59$ in case of $T_t = -20$ °C. This value of the greenhouse forcing must be provided by adding just CO_2 , since the water vapor effect is forbidden by the lack of evaporation. This explains the large value of CO_2 concentration needed in the PlaSim for the transition back from the ice-covered state.

4.3 Radiation: ice margin relation

The latitudinal dependence of the ice line cannot be accounted by the 0-dimensional EBM discussed so far. However, we may formulate a surface energy budget that takes into account this feature including a simple parameterization of heat fluxes. For this purpose, we use the model described in Lindzen (1990):

Fig. 5 Steady solutions of Eq. (5) for the surface temperature T_s as a function of ϵ varying back and forth in the interval 0.2–0.9. The shape of the planetary albedo is specified in Table 2. Arrows denote the direction of variation of ϵ . Units are dimensionless and degree C for ϵ and T_s , respectively

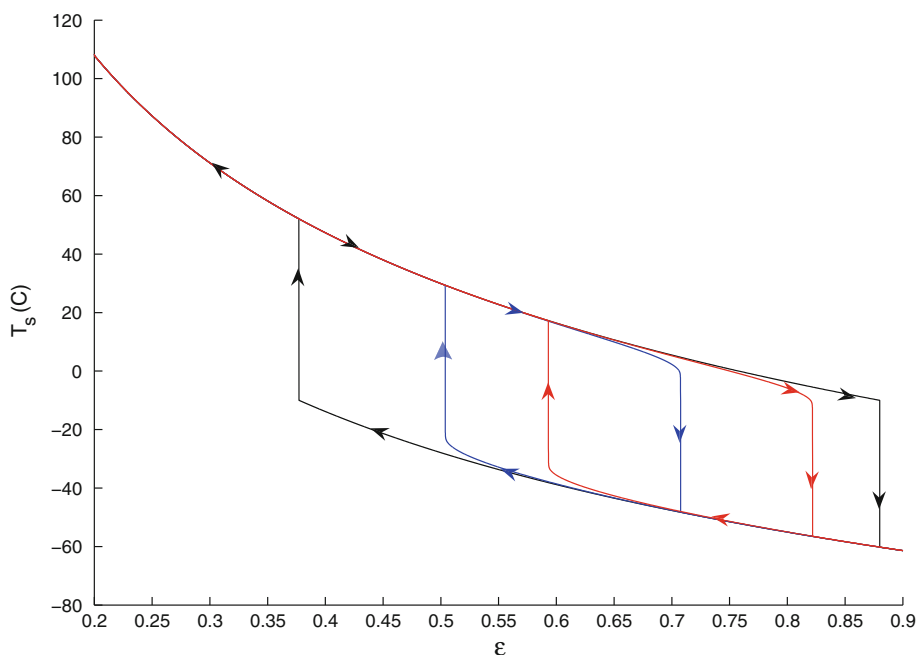


Table 2 The planetary albedo dependence on T_s and on the threshold T_i used for computing the steady states of Eq. (5) as a function of ε (Fig. 5)

| Fig. 5 | T_i (C) | α (Dimensionless) |
|------------|----------------|--|
| Black line | $T_i = -10$ °C | $\alpha = 0.7$ ($T_s > T_i$) $\alpha = 0.3$ ($T_s < T_i$) |
| Blue line | $T_i = -10$ °C | $\alpha = 0.5 + 0.2 \tanh ((T_i - T_s)/10)$ |
| Red line | $T_i = -20$ °C | |

$$C \frac{d}{dt} T_s = S_0 [1 - \alpha(T_s)] - \varepsilon \sigma T_s^4 + F(T_s) \tag{6}$$

with

$$F(T_s) = \beta (T_{sp} - T_s)$$

$$\varepsilon \sigma T_s^4 \cong \varepsilon (A + B T_s)$$

where T_{sp} and β are the global mean surface temperature and the heat-flux coefficient, respectively. Notice that the outgoing long wave flux parameterization consists just in the first two terms of the binomial expansion of T_s^4 around the reference temperature of 273 K; the coefficients A and B are estimated for $\varepsilon = 1$ ($A = 315 \text{ Wm}^{-2}$, $B = 4.6 \text{ Wm}^{-2}\text{C}^{-1}$) and T_s is in degree Celsius. For S_0 we use the annual average as in North (1975):

$$S_0 = \frac{1367}{4} \left(1 - \frac{0.477}{2} (3x^2 - 1) \right), \tag{7}$$

where $x = \sin(\phi)$ with ϕ the latitude.

Let be the ice margin denoted by x_s and $T_s(x_s) = -10$ °C, while $\beta = 2.2 \text{ Wm}^{-2}\text{C}^{-1}$ so that for $\varepsilon = 0.61$ (present climate conditions) $x_s = 0.95$. The planetary albedo is the step function introduced before assuming the values $\alpha_1 = 0.3$ and $\alpha_2 = 0.62$ below and above the ice margin, respectively, while $\alpha(x_s) = (\alpha_1 + \alpha_2)/2$. The value of α_2 has been chosen to be the averaged surface ice albedo in the Northern Hemisphere (NH) for the snowball Earth state as results from the PlaSim simulations.

The global mean surface temperature is given by:

$$T_{sp} = \int_0^1 \left(\frac{S_0(x) (1 - \alpha(x))}{\varepsilon B} - \frac{A}{B} \right) dx \tag{8}$$

Normally, we expect that the ice margin moves towards the equator ($x = 0$) as the radiative forcing ε increases and vice versa. The presence of heat transports should destabilize this unique relationship (ice cap instability) by introducing a critical ice margin x_s^c so that for any $x < x_s^c$ there is only the snowball solution. Thus, we are interested to study the behavior of ε as a function of x_s letting all the other parameters fixed. It turns out that by evaluating Eq. (6) at x_s (with $C = 0$, steady state condition), ε must satisfy the following equation:

$$\Lambda_1 \varepsilon^2 + \Lambda_2 \varepsilon + \Lambda_3 = 0 \tag{9}$$

where the coefficients Λ_i ($i = 1, 2, 3$) are functions of the parameters evaluated at a given x_s . In Fig. 6 (black lines) the solutions of Eq. (9) as a function of x_s are shown in case of $\beta = 0$ (solid line) and $\beta \neq 0$ (dashed line). It is worth noting that for a given x_s , Eq. (9) has two real solutions and the negative one must be excluded since ε is positive defined. From the figure it can be noted that in case of no heat transports for each value of ε ranging in the interval 0.35–0.85 (note roughly the same range identified in Fig. 5, black line, by the bifurcation points) there is a unique value of x_s . When the heat transports are active on the system, they cool the equatorial regions and warm the polar ones. This implies that lower values of ε are enough to allow the ice to advance towards the tropics, while the opposite holds at high latitudes. Moreover, it appears that a critical x_s exists for which the solution is in a snowball state (the ice forms also in the tropics). In our case, x_s^c , which corresponds to the maximum values of ε , is about 0.32, say 18.7 N: this is the critical latitude beyond which the ice extends to the equator. Moreover, it appears that for ε between 0.7 and 0.74 (maximum value) two ice margins satisfy Eq. (9). Since the heat fluxes introduce a critical ice margin so that the ice can form also in the tropics, they can

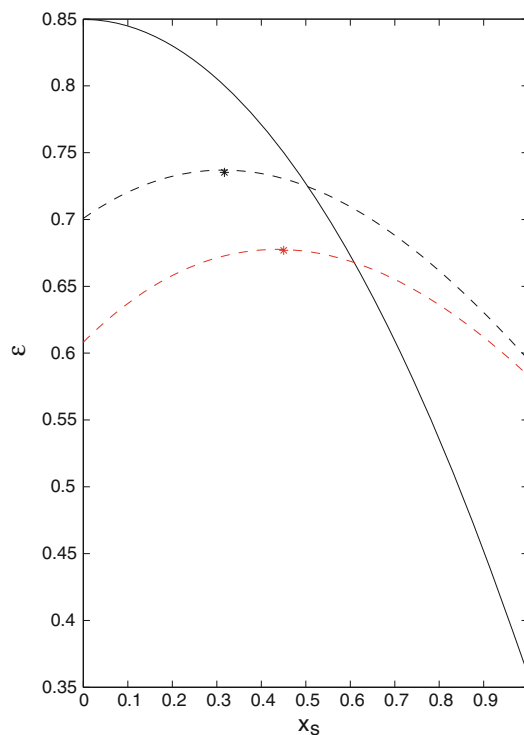


Fig. 6 Radiative forcing ε as a function of the ice margin x_s (solution of Eq. (9)) for $\beta = 0$ and $\alpha_2 = 0.62$ (solid black line), $\beta > 0$ and $\alpha_2 = 0.62$ (dashed black line), $\beta > 0$ and $\alpha_2 = 0.7$ (solid red line). Asterisks denote the maximum of the curves for $\beta > 0$. Units are dimensionless

be considered a key parameter for the transition to snowball state and vice versa.

4.4 Hemispheric asymmetry

Since in the SH the surface albedo of the ice is expected to be higher than in the NH (as supported by the PlaSim simulation when the ice-covered state is reached), let us consider the solution of Eq. (9) with the same heat transports but $\alpha_2 = 0.7$ (red dashed line in Fig. 6). In this case, the range of variability of the radiative forcing associated with the ice margin is reduced and, most importantly, the critical ice margin is changed to $x_5^c = 0.45$, which corresponds to about 26.7 N. This means that the snowball Earth solution is reached more rapidly for a higher value of α_2 because the critical latitude of the ice margin is moved poleward. This explains the asymmetric solution of PlaSim between NH and SH, which is particularly evident when O_3 is removed. Concluding, the origin of the asymmetric response between the NH and SH lies in the different ice albedo of the two hemispheres.

5 Conclusions

In the present paper we have studied the effect of a sudden decrease of atmospheric trace gases that interact with thermal radiation. We found the following:

- If the model has bifurcation points, its behavior depends crucially on the exact amount of the gases' concentrations as long as their effect on water vapor is significant. The climate model used shows the existence of a threshold value for CO_2 concentration leading to the transition to the modern snowball Earth;
- The oceanic Q-flux, although globally averaging to zero, has a crucial role on the thermodynamic state of the planet when a sudden increase in the outgoing infrared radiation is applied on it. A better representation of these fluxes may, however, modify this conclusion;
- The model response of the thermal field has a great degree of simplicity; that is, when long time scales are analyzed, the chaotic nature of the actual solution is averaged out (Held et al. 2010) and only residuals emerge. In this case, a simple energy budget at the surface can account for most of the model response.

It is worth noting that the sensitivity analysis for dynamic systems, supposed to be in a steady state, to small variations of the external forcing would be misleading when the system has a few steady states. In this case, in fact, a small change in the forcing (for example around the CO_2 threshold) could lead to a dramatic change in the

steady state so that the analysis would not be able to capture the complexity of the system response.

Further analyses using a coupled atmosphere–ocean GCM and different parameterizations of clouds should be performed. These will be topics for future studies.

Acknowledgments Support by the Max Planck Society is acknowledged (KF).

References

- Berk A, Bernstein LS, Robertson DC (1989) MODTRAN: A moderate resolution model for LOWTRAN 7. Air Force Geophys Lab, Bedford, MA, Rep GL-TR-89-0122
- Bordi I, Dell'Aquila A, Speranza A, Sutera A (2004) On the midlatitude tropopause height and the orographic-baroclinic adjustment theory. *Tellus* 56A:278–286
- Bordi I, Fraedrich K, Lunkeit F, Sutera A (2007) Tropospheric double-jets, meridional cells and eddies: a case study and idealized simulations. *Mon Weather Rev* 135:3118–3133
- Bordi I, Fraedrich K, Sutera A, Zhu X (2012a) On the climate response to zero ozone. *Theor Appl Climatol* 109:253–259
- Bordi I, Fraedrich K, Sutera A, Zhu X (2012b) Transient response to well-mixed greenhouse gas changes. *Theor Appl Climatol* 109:245–252
- Budyko MI (1969) The effect of solar radiation variations on the climate of the Earth. *Tellus* 21:611–619
- Caldeira K, Kasting JF (1992) Susceptibility of the early earth to irreversible glaciation caused by carbon dioxide clouds. *Nature* 359:226–228
- Crowley TJ, Hyde WT, Peltier WR (2001) CO_2 levels required for deglaciation of a ‘‘Near-Snowball’’ Earth. *Geophys Res Lett* 28:283–286
- Dahms E, Borth H, Lunkeit F, Fraedrich K (2011) ITCZ splitting and the influence of large-scale eddy fields on the tropical mean state. *J Met Soc Japan* 89:399–411
- Dekker SC, de Boer HJ, Brovkin V, Fraedrich K, Wassen MJ, Rietkerk M (2010) Biogeophysical feedbacks trigger shifts in the modelled climate system at multiple scales. *Biogeosciences* 7:1237–1245
- Donnadieu Y, Godd ris Y, Ramstein G, N d lec A, Meert J (2004) A ‘snowball earth’ climate triggered by continental break-up through changes in runoff. *Nature* 428(6980):303–306
- Eliassen E, Machenhauer B, Rasmussen E (1970) On a numerical method for integration of the hydrodynamical equations with a spectral representation of the horizontal fields. Institute of Theoretical Meteorology, University of Copenhagen, Denmark, Rep 2
- Fraedrich K (1978) Structural and stochastic analysis of a zero-dimensional climate system. *Q J R Meteorol Soc* 104:461–474
- Fraedrich K, Lunkeit F (2008) Diagnosing the entropy budget of a climate model. *Tellus* 60A:921–931
- Fraedrich K, Jansen H, Kirk E, Luksch U, Lunkeit F (2005a) The planet simulator: towards a user friendly model. *Meteorol Zeitschrift* 14:299–304
- Fraedrich K, Jansen H, Kirk E, Lunkeit F (2005b) The planet simulator: green planet and desert world. *Meteorol Zeitschrift* 14:305–314
- Garreaud RD, Molina A, Farias M (2010) Andean uplift, ocean cooling and Atacama hyperaridity: a climate modeling perspective. *Earth Planet Sci Lett* 292:39–50
- Green AES (1964) Attenuation by ozone and the earth's albedo in the middle ultraviolet. *Appl Opt* 3:203–208

- Grosfeld K, Lohmann G, Rambu N, Fraedrich K, Lunkeit F (2007) Atmospheric multidecadal variations in the North Atlantic realm: proxy data, observations, and atmospheric circulation model studies. *Clim Past* 3:39–50
- Hartmann DL (1994) *Global physical climatology*. Academic Press, San Diego
- Held IM, Winton M, Takahashi K, Delworth T, Zeng F, Vallis GK (2010) Probing the fast and slow components of global warming by returning abruptly to preindustrial forcing. *J Clim* 23:2418–2427
- Hoffman PF, Kaufman AJ, Halverson GP, Schrag DP (1998) A neoproterozoic snowball earth. *Science* 281(5381):1342–1346
- Hu Y, Yang J (2010) Uncertainty of the CO₂ threshold for melting the hard snowball Earth. *Clim Past* 6:1337–1350
- Kiehl JT, Trenberth KE (1997) Earth's annual global mean energy budget. *Bull Amer Meteorol Soc* 78:197–208
- Kuo HL (1965) On formation and intensification of tropical cyclones through latent heat release by cumulus convection. *J Atmos Sci* 22:40–63
- Kuo HL (1974) Further studies of the parameterization of the influence of cumulus convection on large-scale flow. *J Atmos Sci* 31:1232–1240
- Lacis AA, Hansen KE (1974) A parameterization for the absorption of solar radiation in the Earth's atmosphere. *J Atmos Sci* 31:118–133
- Lacis AA, Schmidt GA, Rind D, Ruedy RA (2010) Atmospheric CO₂: principal control knob governing earth's temperature. *Science* 330:356–359
- Laursen L, Eliassen E (1989) On the effect of the damping mechanisms in an atmospheric general circulation model. *Tellus* 41A:385–400
- Le Hir G, Ramstein G, Donnadieu Y, Pierrehumbert RT (2007) Investigating plausible mechanisms to trigger a deglaciation from a hard snowball earth. *CR Geosci* 339:274–287
- Le Hir G, Donnadieu Y, Krinner G, Ramstein G (2010) Toward the snowball earth deglaciation. *Clim Dyn* 35:285–297
- Lindzen RS (1990) *Dynamics in atmospheric physics*. Cambridge University Press, New York
- Lindzen RS (1995) How cold would we get under CO₂-less sky? *Phys Today* 48:78–80
- Louis JF (1979) A parametric model of vertical eddy fluxes in the atmosphere. *Bound Layer Meteor* 17:187–202
- Louis JF, Tiedke M, Geleyn J-F (1982) A short history of the PBL parameterisation at ECMWF. In: *Proceedings, ECMWF workshop on planetary boundary layer parameterization*, Reading, 25–27 Nov 1981, 59–80
- Lucarini V, Fraedrich K, Lunkeit F (2010) Thermodynamic analysis of snowball earth hysteresis experiment: efficiency, entropy production, and irreversibility. *Q J R Meteorol Soc* 136:2–11
- Marotzke J, Botzet M (2007) Present-day and ice-covered equilibrium states in a comprehensive climate model. *Geophys Res Lett* 34:L16704. doi:10.1029/2006GL028880
- Micheels A, Montenari M (2008) A snowball earth versus a slushball earth: results from neoproterozoic climate modeling sensitivity experiments. *Geosph* 4:401–410
- North GR (1975) Theory of energy-balance climate models. *J Atmos Sci* 32:2033–2043
- Orszag SA (1970) Transform method for calculation of vector coupled sums. *J Atmos Sci* 27:890–895
- Pierrehumbert RT (2005) Climate dynamics of a hard snowball earth. *J Geophys Res* 110:D01111. doi:10.1029/2004JD005162
- Pierrehumbert RT, Abbot DS, Voigt A, Koll D (2011) Climate of the neoproterozoic. *Annu Rev Earth Planet Sci* 39:417–460
- Roeckner E, Arpe K, Bengtsson L, Brinkop S, Dümenil L, Esch M, Kirk E, Lunkeit F, Ponater M, Rockel B, Sausen R, Schlese U, Schubert S, Windelband M (1992) Simulation of the present-day climate with the ECHAM model: Impact of model physics and resolution. *Max-Planck-Institut für Meteorologie, Hamburg, Rep* 93
- Romanova V, Lohmann G, Grosfeld K (2006) Effect of land albedo, CO₂, orography, and oceanic heat transport on extreme climates. *Clim Past* 2:31–42
- Rondanelli R, Lindzen RS (2010) Can thin cirrus clouds in the tropics provide a solution to the faint young Sun paradox? *J Geophys Res* 115:D02108. doi:10.1029/2009JD012050
- Roscher M, Stordal F, Svensen H (2011) The effect of global warming and global cooling on the distribution of the latest Permian climate zones. *Palaeogeogr Palaeoclimatol Palaeoecol* 309:186–200
- Saltzman B, Sutera A (1984) A model of the internal feedback system involved in late quaternary climatic variations. *J Atmos Sci* 41:736–745
- Sasamori T (1968) The radiative cooling calculation for application to general circulation experiments. *J Appl Meteorol* 7:721–729
- Schmittner A, Silva TAM, Fraedrich K, Kirk E, Lunkeit F (2011) Effects of mountains and ice sheets on global ocean circulation. *J Clim* 24:2814–2829
- Sellers WD (1969) A global climatic model based on the energy balance of the earth-atmosphere system. *J Appl Meteor* 8:392–400
- Semtner AJ Jr (1976) A model for the thermodynamic growth of sea ice in numerical investigations of climate. *J Phys Oceanogr* 3:379–389
- Slingo A, Slingo JM (1991) Response of the national center for atmospheric research community climate model to improvements in the representation of clouds. *J Geophys Res* 96:341–357
- Stenzel O, Grieger B, Keller HU, Greve R, Fraedrich K, Lunkeit F (2007) Coupling planet simulator Mars, a general circulation model of the Martian atmosphere, to the ice sheet model SICOPOLIS. *Planet Space Sci* 55:2087–2096
- Stephens GL (1978) Radiation profiles in extended water clouds. II: parameterization schemes. *J Atmos Sci* 35:2123–2132
- Stephens GL, Ackermann S, Smith EA (1984) A shortwave parameterization revised to improve cloud absorption. *J Atmos Sci* 41:687–690
- Sutera A (1981) On stochastic perturbation and long-term climate behaviour. *Q J R Meteorol Soc* 107:137–151
- Trenberth KE, Smith L, Qian T, Dai A, Fasullo J (2006) Estimates of the global water budget and its annual cycle using observational and model data. *J Hydrometeorol* 8:758–769
- Voigt A, Marotzke J (2010) The transition from the present-day climate to a modern snowball Earth. *Clim Dyn* 35:887–905
- Winton M (2003) On the climatic impact of ocean circulation. *J Clim* 16:2875–2889
- Zhu X, Fraedrich K, Blender R (2006) Variability regimes of simulated Atlantic MOC. *Geophys Res Lett* 33:L21603. doi:10.1029/2006GL027291
- Zhu X, Fraedrich K, Liu Z, Blender R (2010) A demonstration of long term memory and climate predictability. *J Clim* 23:5021–5029
- Zhu X, Bothe O, Fraedrich K (2011) Summer atmospheric bridging between Europe and East Asia: influences on drought and wetness on the Tibetan Plateau. *Quat Int* 236:151–157